

Electrochemical Promotion of Ammonia Synthesis with Proton-Conducting Solid Oxide Fuel Cells

Chien-I Li¹, Akio Oikawa¹, Fumihiko Kosaka², Junichiro Otomo^{*1}

¹Department of Environment Systems, Graduate School of Frontier Sciences, The University of Tokyo, 5-1-5 Kashiwanoha, Kashiwa, Chiba 277-8563, Japan

²Research Institute of Energy Frontier, Department of Energy and Environment, Research Institute of Energy Frontier, AIST Tsukuba West, 16-1 Onogawa, Tsukuba, Ibaraki 305-8569, Japan

*Corresponding author: E-mail: otomo@k.u-tokyo.ac.jp

Received: 23 August 2018, Revised: 11 December 2018 and Accepted: 15 December 2019

DOI: 10.5185/amlett.2019.2259

www.vbripress.com/aml

Abstract

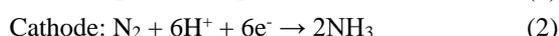
Direct electrochemical synthesis of ammonia was performed using proton-conducting solid oxide fuel cells. In this study, we investigated the effect of electrode potential on the reaction kinetics of ammonia formation with Fe- and Ru-based catalysts in detail. The cell configuration was Pt|BaCe_{0.9}Y_{0.1}O₃ (BCY)|K-modified Fe or Ru-BCY. The ammonia formation rate of K-Ru was higher than that of K-Fe at the rest potential. However, the ammonia formation rate significantly increased by cathodic polarization for the Fe catalyst, and it showed a linear increase for the Ru catalyst, i.e., the ammonia formation rate for K-Fe significantly increased from the rest potential by several hundred times to -1.2V at 700°C, but K-Ru showed only five times increase. The results suggest that the addition of K into Fe-BCY and cathodic polarization can improve the ammonia formation rate because of the promotion of bond dissociation of the N molecule on the Fe catalyst. The present work provides a hint for efficient ammonia formation and contribute to further development of ammonia electrochemical synthesis with proton-conducting solid oxide fuel cells. Copyright © VBRI Press.

Keywords: Ammonia synthesis, proton conductor, electrochemical promotion, energy storage.

Introduction

Currently, investigations of alternatives to carbon-based liquid fuels and hydrogen carriers are crucial challenges in the world. Ammonia is a carbon-free fuel and a promising green energy carrier and means of storage of hydrogen because it has high energy density and can be liquefied easily [1]. Nowadays, ammonia is predominantly synthesized via an industrial Haber-Bosch process. In this process, the reactions occur via Fe-based catalysts at high temperature and pressure from N₂ and H₂, which consumes massive amounts of energy and releases a large amount of CO₂ [2]. Ru-based catalysts have also been discussed because its catalytic reaction is better than that of Fe-based catalysts [2]. The additions of Al and K could improve the performance of ammonia synthesis [2].

In the past decade, there have been many studies on the direct electrochemical synthesis of ammonia at low temperature [3-12], intermediate temperature [13-18] and high temperature [19-29]. The reaction at the anode is water or hydrogen decomposition to form protons and oxygen and emitted electron (Eq. 1). At the cathode, the produced protons diffusing through electrolyte and electrons react with N₂ to form NH₃ (Eq. 2). The total reaction is described in Eq. 3.



Among these papers, one reported the electrochemical synthesis of ammonia using a Fe catalyst at low temperature [3]. The authors reported a very high faradaic efficiency of approximately 41% but a low ammonia formation rate of $3.8 \times 10^{-12} \text{ mol s}^{-1} \text{ cm}^{-2}$ at 50°C. In addition to Fe-based catalysts, Ru catalyst have also been explored for improving the ammonia formation rate. In the previous study [17], the result indicated that ammonia electrochemical synthesis using Ru at approximately 250 °C showed a high ammonia yield of approximately $1 \times 10^{-11} \text{ mol s}^{-1} \text{ cm}^{-2}$ with a faradaic efficiency of 0.05%. At temperatures higher than 500°C, proton conductors based on perovskite materials such as BaCe_{1-x-y}Zr_yY_xO_{3-δ} (BCZY) were dominant because of significant proton conductivity. Many papers have reported ammonia electrochemical synthesis above 500°C with a variety of electrode catalysts such as Ni [20], Fe [22, 27], Ru [24-26], Ag [29] and Pt [29]. However, the mechanism of the effect of cathodic polarization on ammonia formation rate has not been clarified.

Recently, we reported the electrochemical promotion of ammonia synthesis using proton-conducting solid oxide fuel cells using Fe-based and Ru-based electrode catalysts [22, 25]. It was observed that Ru nanoparticles 1-10 nm in diameter formed on BCY and $\text{La}_{0.3}\text{Sr}_{0.6}\text{TiO}_3$ (LST) surfaces after appropriate treatment for reduction of the electrodes [25]. The results revealed that the electrochemical synthesis of ammonia using Ru-doped BCY was better than that using Ru-doped (LST) under pure N_2 atmosphere. Because of high proton conductivity of BCY, greater numbers of protons and electrons could be transported to Ru on BCY surface to react with adsorbed nitrogen to form ammonia.

In our recent study, we reported improved ammonia electrochemical synthesis using K-Al-Fe-BCY with the infiltration method [22]. We observed that the ammonia formation rate under $\text{H}_2\text{-N}_2$ atmosphere was higher than that under pure N_2 atmosphere. The paper also indicated that the electrochemical synthesis of ammonia could be greatly promoted by the infiltration of K into Fe-based electrode catalysts and cathodic polarization [2, 22].

In this study, the electrochemical synthesis of ammonia was studied with K-Fe-BCY and K-Ru-BCY cathodes by the infiltration method. To the best of our knowledge, Ru-based catalysts are the best catalysts for ammonia synthesis [2]. Thus, the electrochemical synthesis of ammonia using a Ru-based catalyst was investigated and compared to that of a Fe-based catalyst.

This paper reports on the preparation of the electrodes and the observations of ammonia electrochemical synthesis. First, electrode structures were prepared by the infiltration method and observed. Second, the effects of the amounts of K addition into Fe-based and Ru-based cathodes on the performance of electrochemical synthesis were examined. Finally, the reaction mechanisms of electrochemical synthesis of ammonia on K-Ru-BCY and K-Fe-BCY are discussed.

Experimental

Material synthesis and characterization

BCY powders were synthesized by the coprecipitation method with metal nitrate precursors, $\text{Ba}(\text{NO}_3)_2$ (purity: 99.99%, Kanto Chemical Co., Inc., Japan), $\text{Ce}(\text{NO}_3)_3 \cdot 6\text{H}_2\text{O}$ (purity: 99.99%, Kanto Chemical Co., Inc., Japan) and $\text{Y}(\text{NO}_3)_3 \cdot 6\text{H}_2\text{O}$ (purity: 99.99%, Kanto Chemical Co., Inc., Japan), which were stoichiometrically dissolved in water. $(\text{NH}_4)_2(\text{COO})_2$ (Kanto Chemical Co. Inc., Japan), whose concentration was 1.5 times higher than the total cation concentration, was used as a precipitant. Then, the precipitate was filtered with suction filtration, precalcined at 800°C , and then calcined at 1200°C in air to form BCY powder.

BCY pellets were prepared using uniaxial pressing and subsequent cold isostatic pressing. BCY powder (1.5 g) was first uniaxially pressed under 1 t cm^{-2} and then isostatically pressed under 180 MPa. Next, the BCY pellets were calcined at 1600°C in air with sacrificial powder of BCY to prevent intermixing with crucible and vaporization of barium.

Cell fabrication

A porous BCY electrode on BCY electrolyte was fabricated by the doctor-blade method. The BCY powder was mixed with α -terpineol (solvent), ethyl cellulose (binder), sorbitan sesquioleate (dispersant), dibutyl phthalate (plasticizer), and poly methyl methacrylate resin (pore-formation) to form a slurry. The slurry was then pasted onto the BCY electrolyte and calcined at 1300°C . Finally, the counter electrode and reference electrode were attached on the BCY electrolyte pellets by coating the pellets Pt paste (Tanaka Kikinzoku Kogyo K. K., Japan), which were then annealed at 900°C in 3% H_2 atmosphere for 3h, as shown in Fig. 1a.

K-Fe-BCY and K-Ru-BCY cathodes were fabricated by the impregnation method. For K-Fe-BCY, KNO_3 (purity: 99.99%, Kanto Chemical Co., Inc., Japan) and $\text{Fe}(\text{NO}_3)_3 \cdot 9\text{H}_2\text{O}$ (purity: 99.99%, Wako Chemical Co., Inc., Japan) as precursors were each dissolved in water to form 2M solution. First, the iron nitrate solution was poured onto the BCY cathode until the solution filled the pore volume of the BCY cathode. The sample was then placed in a vacuum chamber for 5 min and then put in a 90°C oven for 5 min to remove the extra water. The above processes were carried out several times until the Fe reached the desired weight ratio. Finally, the sample was pre-annealed at 700°C for 1h in air. The above process was repeated for the KNO_3 solution until the K wt.% reached a specific amount. The obtained samples were then annealed at 900°C for 1h in 3% H_2 . The same process was also used to fabricate K-Ru-BCY with 0.5M $\text{Ru}(\text{NO}_3)_3$ (purity: 99.9%, Furuya Metal Co., Inc., Japan) and KNO_3 . K-Ru-BCY and K-Fe-BCY samples were characterized using a scanning electron microscope (SEM, JEOL JSM-5600, Japan), S4700 (Hitachi, Japan), and X-ray diffraction (XRD, SmartLab, RIGAKU, Japan).

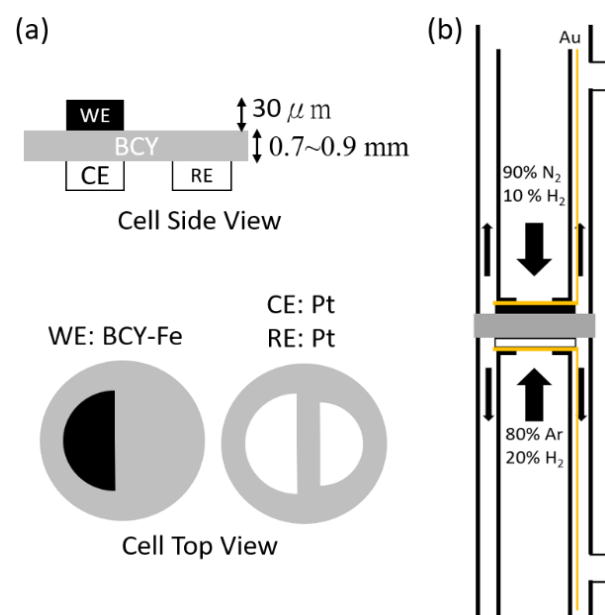


Fig. 1. Schematic images of single cell for the electrochemical measurement for the ammonia synthesis.

Electrochemical synthesis of ammonia

Ammonia electrosynthesis was performed using a single cell of K-Fe-BCY (K-Ru-BCY) | BCY | Pt at 700°C with a dry gas mixture of 10 %H₂-90% N₂ and wet gas composed of 20% H₂-80% Ar flowing into the WE and CE, respectively, as shown in Fig. 1b. AC impedance measurements were performed from 10⁻²-10⁵ HZ using an Autolab PGSTAT128N (Metrohm Autolab B.V., Netherlands). The IR-loss was corrected by the applied voltage minus the times of current and resistance of the electrolyte. The ammonia formation was captured by flowing the outlet gas from the WE side into 0.01 mM H₂SO₄ solution and then the solution was analyzed by ion chromatography (EXTREMA, Jasco, Japan).

Results and discussion

Characterizations

To characterize the crystal phases in the K-Fe-BCY and K-Ru-BCY electrodes, XRD was adopted to observe the phase. Fig. 2 shows the XRD patterns of K-Ru-BCY and K-Fe-BCY after annealing at 900°C in 3% H₂/Ar. For K-Ru-BCY, the XRD patterns show strong peaks of BCY phase and weak those of Ru phase (Fig. 2a). However, the XRD patterns for K-Fe-BCY showed only the peaks of BCY phase (Fig. 2b). Fe phase could not be observed because of the small amounts of Fe.

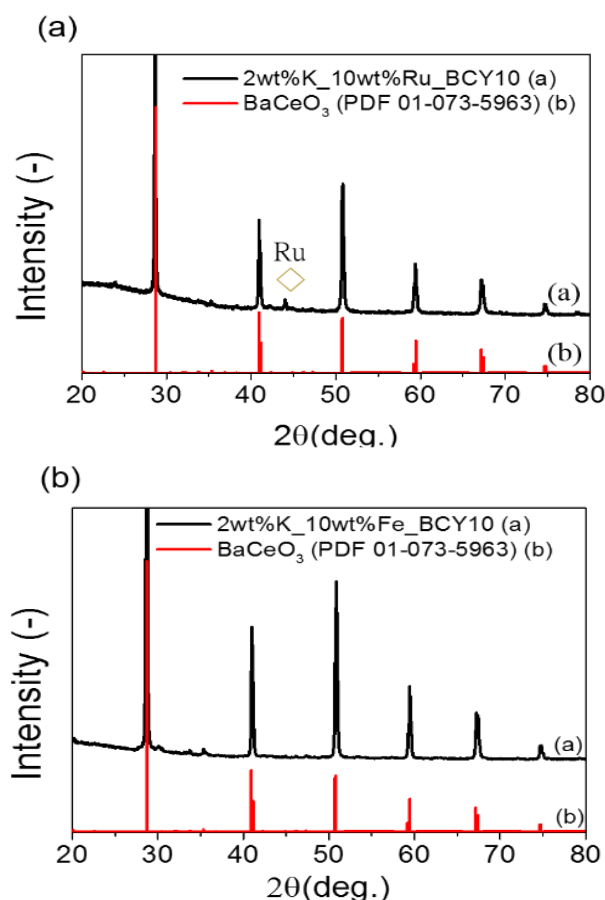


Fig. 2. XRD patterns of (a) Ru-infiltrated BCY and (b) Fe-infiltrated BCY cathodes after reduction at 900°C in 3%H₂/Ar.

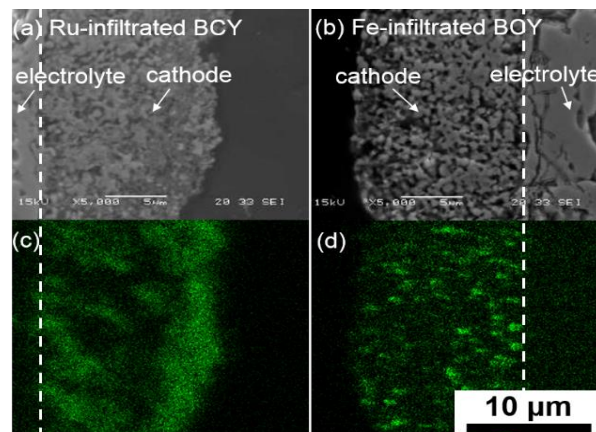


Fig. 3. Cross-sectional SEM images and EDX-mapping of (a), (c) Ru-infiltrated BCY and (b), (d) Fe-infiltrated BCY cathodes.

The distribution of Ru and Fe in the BCY electrode was investigated by SEM-EDX, shown in Fig. 3. Figs. 3a and 3b are the cross-sectional images of the Ru-BCY and Fe-BCY electrodes, respectively, after annealing at 900°C in 3%H₂/Ar, and Figs. 3c and 3d are the EDX mappings of Ru and Fe, respectively. The thickness of the porous electrode was approximately 10 μm for both electrodes. However, the intensity of Ru near the electrode surface and at the interface between the electrolyte and the electrode was greater than that for internal Ru-BCY, which indicated Ru particles accumulated on the electrode surface and interface (Fig. 3c). However, Fig. 3d exhibited good distribution of Fe in the electrode.

In order to further understand the sizes of the Fe and Ru particles, field emission (FE)-SEM was used to obtain the cross-sectional images of Fe-BCY and Ru-BCY. Fig. 4a shows cross-sectional image of the BCY electrode, where the size of the BCY particles was larger than 200 nm. Fig. 4b shows many small iron particles approximately 50 nm in size on the BCY surface. As compared to Fe-BCY, Ru-BCY exhibited small sparse particles on the BCY surface because of the higher density of Ru (Ru density: 12.45 g/cm³, Fe density: 6.98 g/cm³), resulting in a lower volume, as shown in (Fig. 4c).

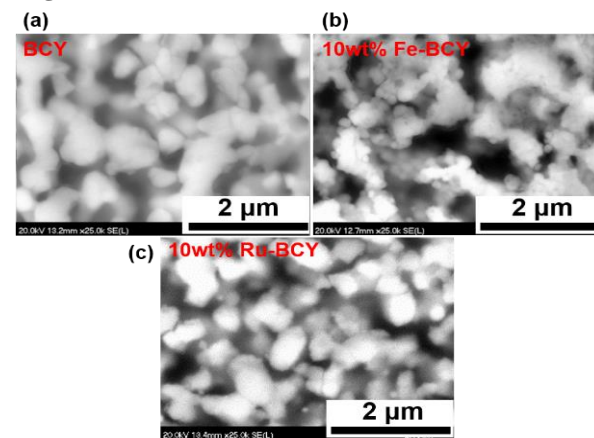


Fig. 4. Cross-sectional SEM images of (a) porous BCY cathode (i.e., before Fe(Ru) infiltration), (b) Fe-infiltrated BCY cathode and (c) Ru-infiltrated BCY cathode.

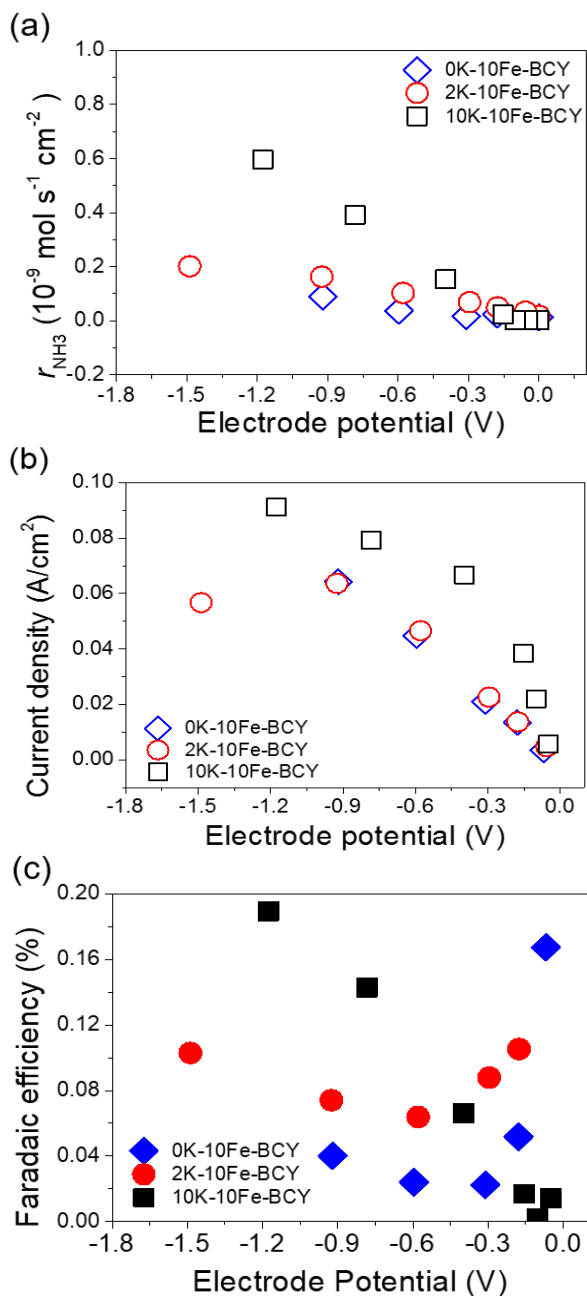


Fig. 5. (a) Ammonia formation rates for K-Fe-BCY at 700°C and (b) current density and (c) faradaic efficiency on the Fe-infiltrated BCY cathodes with different K-additions (*i*R-corrected) (working electrode: 10% H₂/90% N₂ and counter electrode: 2% H₂O/20% H₂/78% Ar).

Effects of K-Addition into Fe-BCY on ammonia formation rate

Fig. 5 shows the ammonia formation rate for the K-Fe-BCY|BCY|Pt cell at 700°C with different applied voltages. 2% H₂O/20% H₂/78% Ar was fed to the anode side while 10% H₂/90% N₂ was fed to the cathode side. Hereafter, the convention (shorthand, formula) *x*K-*y*Fe(Ru)-BCY is used, where *x* indicates the weight percent (wt.%) of K and *y* indicates the weight percent of Fe(Ru) in the BCY electrode. **Fig. 5a** shows the ammonia formation rates of 0K-, 2K- and 10K-10Fe-BCY electrodes. The results exhibited the lower performances for ammonia formation rates from

1.8×10^{-12} to $1.9 \times 10^{-11} \text{ mol s}^{-1} \text{ cm}^{-2}$ at the rest potential (i.e., current density = 0). However, it was clearly observed that the electrochemical promotion of ammonia synthesis increased with increasing amounts of K-addition. The formation rate of ammonia for 10K-10Fe-BCY significantly increased from 1.79×10^{-12} at the rest potential to $5.96 \times 10^{-10} \text{ mol s}^{-1} \text{ cm}^{-2}$ at -1.2V, an increased by 330 times. However, for 0K- and 2K-10Fe-BCY, the formation rate increased by 6.9 and 10 times, respectively. These results indicated that ammonia formation rate for K-Fe-BCY had a highly positive relation to cathodic polarization, and the amount of K-addition also showed a positive effect on the ammonia formation rate. These results agreed with those of the previous study of K and Al-modified Fe-BCY catalyst [22]. As a possible mechanism, we presumed that the acceleration of the ammonia formation rate resulted from the lower work function induced by the addition of K, which could promote bond dissociation of N₂ adsorbed on Fe to form N atoms on the catalyst surface.

Figs. 5b and **5c** show current density and corresponding faradaic efficiency of ammonia formation. The faradaic efficiencies for 2K-10Fe-BCY and 0K-10Fe-BCY decreased with increasing cathodic polarization, whereas that for 10K-10Fe-BCY exhibited an increase of the faradaic efficiency with increasing cathodic polarization. This was significant evidence that the ammonia formation rate was strongly influenced by the K addition, as well as by cathodic polarization. However, all K-Fe-BCY electrode catalysts showed lower faradaic efficiencies of the ammonia formation rate below 0.3%. The results demonstrated that the performance of ammonia electrosynthesis could be modified by K addition into Fe based cathode, but a large amount of hydrogen was also produced in the electrochemical reaction.

Fig. 6a shows the ammonia formation rate with the K-Ru-BCY|BCY|Pt cell at 700°C. The ammonia formation rates at the rest potential for 2K-10Ru-BCY and 10K-10Ru-BCY were approximately 9.51×10^{-11} and $1.24 \times 10^{-10} \text{ mol s}^{-1} \text{ cm}^{-2}$, respectively, which was higher than that for K-Fe-BCY at the rest potential. However, the effect of cathodic polarization on the ammonia formation rate for K-Ru-BCY was weaker than that for K-Fe-BCY, i.e., the ammonia formation rate increased by only 4.5 times for both 2K- and 10K-10Ru-BCY. As shown in **Fig. 6b**, the current densities of 2K- and 10K-10Ru-BCY were almost the same as that of 10K-10Fe-BCY. The faradaic efficiency of K-Ru-BCY reached approximately 1%, which was much higher than that of K-Fe-BCY. However, the faradaic efficiency gradually decreased because the high faradaic efficiency originated from catalytic reaction rather than from the electrochemical reaction of ammonia formation. The results suggest that the amounts of K addition into Ru-BCY had a weaker effect in terms of the ammonia formation rate and the faradaic efficiency. Also, K-Ru-BCY showed better performance of catalytic reaction than K-Fe-BCY, whereas K-Fe-BCY was influenced significantly by cathodic polarization.

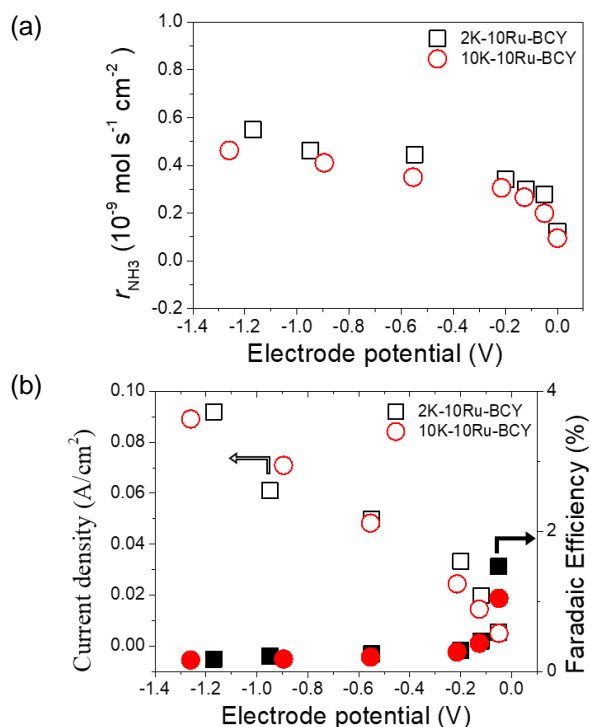


Fig. 6. (a) Ammonia formation rates for K-Ru-BCY at 700°C and (b) current density and faradaic efficiency on the Ru-infiltrated BCY cathodes with different K-additions (*iR*-corrected) (working electrode: 10% H₂/90% N₂ and counter electrode: 2% H₂O/20% H₂/78% Ar). Filled and open symbol represented faradaic efficiency and current density, respectively.

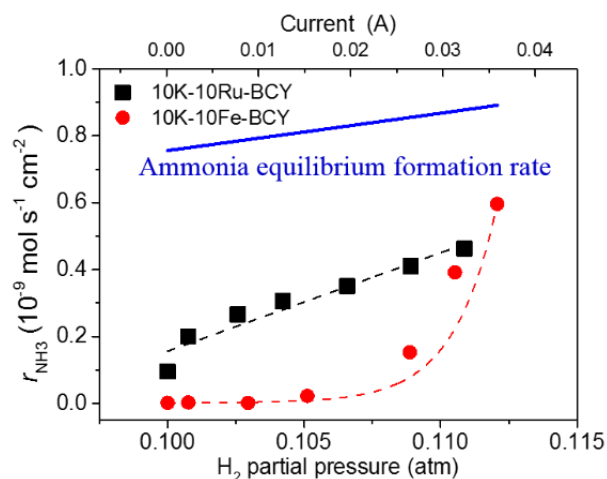


Fig. 7. Ammonia formation rate vs hydrogen partial pressure. The blue dash line was ammonia equilibrium formation rate at different H₂ partial pressure.

Ammonia formation rate for K-Fe-BCY and K-Ru-BCY

The different effects of cathodic polarization on the ammonia formation rate for K-Ru-BCY and K-Fe-BCY were observed. **Fig. 7** suggests that the comparison of the ammonia formation rate depends on hydrogen partial pressure for 10K-10Ru-BCY and 10K-10Fe-BCY. At the rest potential, the H₂ partial pressure was 0.1 atm. With increasing cathodic potential, the H₂ partial pressure and current density increased because of H⁺ pumping from the anode (Eq. 4).



The solid line in **Fig. 7** indicated the equilibrium formation rate of ammonia under specific hydrogen and nitrogen partial pressures at 700°C.

From **Fig. 7**, a linear increase of the ammonia formation rate for 10K-10Ru-BCY and a significant increase for 10K-10Fe-BCY were observed.

Here, first we consider the ammonia formation from the catalytic reaction (indirect path). The reactions are as follows:

Indirect path:



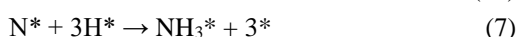
where * and i* are active sites on the surface and adsorbed species, respectively. The ammonia formation rate for 10K-10Ru-BCY was higher than that of 10K-10Fe-BCY at the rest potential, which suggested that 10K-10Ru-BCY had better catalytic performance for N₂ bond dissociation (Eq. 6) than 10K-10Fe-BCY. With increasing cathodic potential, the ammonia formation rate exhibited a linear increase from 9.51×10^{-11} to 5.50×10^{-10} mol s⁻¹ cm⁻² for Ru-BCY. In terms of the indirect path, we considered the reaction rate using the following equation (Eq. 9):

$$r_{\text{NH}_3} = k[\text{H}_2]^\alpha[\text{N}_2]^\beta, \quad (9)$$

where *k*, *α* and *β* were the reaction constant and the reaction orders for hydrogen and nitrogen, respectively. The reported value of the reaction order of H₂, *α*, is approximately -1 to 0 in standard Ru-based catalysts [28]. The negative values indicate that there was dissociative adsorption of H₂ on Ru, which prevented N₂ adsorption and consequent dissociation, which has been called hydrogen poisoning on Ru [28]. However, we found that the *α* value was approximately 12 for 10K-10Ru-BCY, which is much larger than that of the standard Ru-based catalysts. Therefore, the increase of the ammonia formation rate cannot be explained by only the indirect path. The same result was also observed for 10K-10Fe-BCY. When the observed values of the ammonia formation rate, in which the hydrogen partial pressure was between 0.109 and 0.112 atm, were used to obtain the reaction order for hydrogen *α*, we obtained *α* = 47. This value was much larger than the reported value, 0.76, for the catalytic reaction [30].

Next, we considered the possibility of direct electrochemical reaction of ammonia formation (i.e., direct path) as follows:

Direct path:



The electrochemical reaction path included NH* and N*, followed by N₂ dissociation reaction (Eq. 10). A rate-determining step in the catalytic reaction was

probably due to N₂ bond dissociation, whereas there was another promoting mechanism for N₂ bond dissociation to form NH* and N* in the direct path. Therefore, the linear increase for 10K-10Ru-BCY might have resulted from not only a strong catalytic reaction but also weak electrochemical promotion in the ammonia synthesis. However, the ammonia formation rate for 10K-10Fe-BCY exhibited a significant increase, which originated from strong influence of cathodic polarization. Furthermore, upon applying a high cathodic potential, a higher ammonia formation rate for 10K-10Fe-BCY than for 10K-10Ru-BCY was observed, which implies that electrochemical promotion for 10K-10Fe-BCY was stronger than that for 10K-10Ru-BCY. The highest ammonia formation rate for 10K-10Fe-BCY and 10K-10Ru-BCY reached 67% and 53% of ammonia equilibrium formation rate, respectively. The reaction product of ammonia might decompose to form N₂ and H₂ because the reverse reaction of ammonia decomposition can proceed on Fe and Ru catalysts. Conclusively, the promotion of ammonia formation rate is affected by catalyst material and cathodic polarization in this study. 10K-10Ru-BCY exhibited a better catalytic reaction but a weak electrochemical reaction, whereas 10K-10Fe-BCY showed a negligible catalytic reaction and a significant promotion by cathodic polarization. We believe that these results may relate to N₂ dissociation induced by cathodic polarization. However, both K-Fe-BCY and K-Ru-BCY exhibited over 50% of ammonia equilibrium formation rate and induced the serious reverse reaction from ammonia to hydrogen and nitrogen. This is our future challenge.

Conclusion

In this study, the electrochemical synthesis of ammonia was conducted using K-Fe-BCY(K-Ru-BCY)|BCY|Pt cells at 700°C, supplying a 90%N₂-10%H₂ gaseous mixture to a cathode side. A low ammonia formation rate for 10K-10Fe-BCY was observed at the rest potential, whereas the performance for 10K-10Ru-BCY exhibited a high catalytic reaction. However, with increasing cathodic polarization, the ammonia formation rate dramatically increased by 330 times with 10K-10Fe-BCY, but that with 10K-10Ru-BCY increased only by 4.5 times, which showed that the effect of cathodic polarization for 10K-10Fe-BCY were stronger than those for 10K-10Ru-BCY. Furthermore, the faradaic efficiency for 10K-10Fe-BCY increased with increasing cathodic polarization, which also strongly supports this result. Conclusively, for 10K-10Ru-BCY, the increase of ammonia formation rate resulted from the increase of H₂ partial pressure and weak electrochemical reaction. However, for 10K-10Fe-BCY, a significant increase of ammonia formation rate was observed resulting from a very strong electrochemical reaction. These results suggest that not only the lower work function of the K addition but also the applied cathodic polarization promoted the N₂ adsorption and dissociation to N* and NH*. These results could reveal the catalyst activity and

electrochemical effects on ammonia formation for K-Ru-BCY and K-Fe-BCY. To investigate further, the mechanism of electrochemical promotion of ammonia formation should be clarified with additional approaches such as spectroscopic technique and isotopic analysis.

Acknowledgements

The authors thank CREST, Japan Science and Technology Agency (JPMJCR1441) for financial support and the Materials Design and Characterization Laboratory, Institute for Solid State Physics, The University of Tokyo for use of SEM and XRD facilities.

References

1. Miura D.; Tezuka T.; *Energy*, **2014**, 68, 428.
2. Liu H. (Ed.); *Ammonia Synthesis Catalysts*; Elsevier B.V.: USA, **2013**.
3. Renner J. N.; Greenlee L. F.; Ayres K. E.; Herring A. M.; *Electrochem. Soc. Interface*, **2015**, 24, 51.
4. Chen S.; Perathoner S.; Ampelli C.; Mebrahtu C.; Su D.; Centi G.; *ACS Sustainable Chem. Eng.*, **2017**, 5, 7393.
5. Chen S.; Perathoner S.; Ampelli C.; Mebrahtu C.; Su D.; Centi G.; *Angew. Chem. Int. Ed.*, **2017**, 56, 2699.
6. Chen G. F.; Cao X.; Wu S.; Zeng X.; Ding L.; Zhu M.; Wang H.; *J. Am. Chem. Soc.*, **2017**, 139, 9771.
7. Zhao X.; Yin F.; Liu N.; Li G.; Fan T.; Chen B.; *J. Mater. Sci.*, **2017**, 52, 10175.
8. Zhou F.; Azofra L. M.; Al-Agele M.; Kar M.; Simonov A. N.; McDonnell-Worth C. J.; Sun C.; Zhang X.; MacFarlane D.; *Energy Environ. Sci.*, **2017**, 10, 2516.
9. Shi M. M.; Bao D.; Wulan B. R.; Li Y. H.; Zhang Y. F.; Yan J. M.; Jiang Q.; *Adv. Mater.*, **2017**, 29, 1606550.
10. Bao D.; Zhang Q.; Meng F.; Zhong H.; Shi M.; Zhang Y.; Yan J. M.; Jiang Q.; Zhang X.-B.; *Adv. Mater.*, **2017**, 1604799.
11. Mukherjee S.; Cullen D. A.; Karakalos S.; Liu K.; Zhang H.; Zhao S.; Xu H.; More K. L.; Wang G.; Wu G.; *Nano Energy*, **2018**, 48, 217.
12. Sheets B. L.; Botte G. G.; *Chem. Commun.*, **2018**, 54, 4250.
13. Kim K.; Yoo C. Y.; Kim J. N.; Yoon H. C.; Han J. I.; *Korean J. Chem. Eng.*, **2016**, 33, 1777.
14. Qing G.; Kikuchi R.; Kishira S.; Takagaki A.; Sugawara T.; Oyama S. T.; *J. Electrochem. Soc.*, **2016**, 163, E282.
15. Bicer Y.; Dincer I.; *J. Electrochem. Soc.*, **2017**, 164, H5036.
16. Qing G.; Sukegawa K.; Kikuchi R.; Takagaki A.; Oyama S. T.; *J. Appl. Electrochem.*, **2017**, 47, 803.
17. Kishira, S.; Qing, G.; Suzu, S.; Kikuchi, R.; *Int. J. Hydrogen Energy*, **2017**, 42, 26843.
18. Imamura K.; Kubota J.; *Sustainable Energy Fuels*, **2018**, 2, 1278.
19. Shimoda N.; Kobayashi Y.; Kimura Y.; Nakagawa G.; Satokawa S.; *J. Ceram. Soc. Jpn.*, **2017**, 125, 252.
20. Vasileiou E.; Kyriakou V.; Garagounis I.; Vourros A.; Manerino A.; Coors W. G.; Stoukides M.; *Solid State Ionics*, **2016**, 288, 357.
21. Amar I. A.; Lan R.; Petit C. T. G.; Tao S.; *Electrocatalysis*, **2015**, 6, 286.
22. Kosaka F.; Nakamura T.; Oikawa A.; Otomo J.; *ACS Sustainable Chem. Eng.*, **2017**, 5, 10439.
23. Wang W. B.; Cao X. B.; Gao W. J.; Zhang F.; Wang H. T.; Ma G. L.; *J. Membr. Sci.*, **2010**, 360, 397.
24. Kosaka F.; Noda N.; Nakamura T.; Otomo J.; *J. Mater. Sci.*, **2017**, 52, 2825.
25. Kosaka F.; Nakamura T.; Otomo J.; *J. Electrochem. Soc.*, **2017**, 164, F1323.
26. Skodra A.; Stoukides M.; *Solid State Ionics*, **2009**, 180, 1332.
27. Ouzounidou M.; Skodra A.; Kokkofitis C.; Stoukides M.; *Solid State Ionics*, **2007**, 178, 153.
28. Kitano M.; Kanbara S.; Inoue Y.; Kuganathan N.; Sushko P.V.; Yokoyama T.; Hara M.; Hosono H.; *Nat. Commun.*, **2015**, 6, 6731.
29. Yun D. S.; Joo J. H.; Yu J. H.; Yoon H. C.; Kim J.N.; Yoo C.Y.; *J. Power Sources*, **2015**, 284, 245.
30. Strongin D. R.; Somorjai G. A.; *J. Catal.*, **1988**, 109, 51.